Solid State Phenomena
ISSN: 1662-9779, Vol. 327, pp 65-70
doi:10.4028/www.scientific.net/SSP.327.65

Submitted: 2021-04-29
Revised: 2021-06-23
Accepted: 2021-07-01
Online: 2022-01-10

Role of Iron-Rich Phases and Porosity on the Ductility of Rheocast Al-Mg-Si-Alloys

Qing Zhang[1,a], Stefan Jonsson[2,b], Arne Dahle[1,c] and Anders E. W. Jarfors[1,d]

[1]Jönköping University, School of Engineering, Materials and Manufacturing, Box 1026, 55111 Jönköping, Sweden

[2]Royal Institute of Technology, Department of Materials science, 1044 Stockholm, Sweden

[a]qing.zhang@ju.se, [b]jonsson@kth.se, [c]arne.dahle@ju.se, [d]anders.jarfors@ju.se

Keywords: Semi-solid casting, Intensive stirring, Segregation, Porosity, Fe-rich intermetallic, Elongation.

Abstract. Treatment of the slurry is important during RheoMetal^{TM} casting. In this work, semi-solid slurries were prepared under different stirring intensities, using two types of stirrers: a naked rod (for regular stirring) and a rod with two blades (for intensive stirring). Tensile tests were performed, investigating fracture surfaces, as well as metallographic samples. The results show that intensive stirring produces castings with finer primary particles and a more homogeneous microstructure. On the other hand, more faceted Fe-rich phases are found along the α-Al grains boundary, due to the dissolution of Fe from the stirrers. Moreover, for intensive stirring castings, the porosity found on the fracture surfaces are smaller, while more second (intermetallic) phases, especially Fe-rich phases, are observed. Consequently, the castings with intensive stirring show worse ductility. Finally, a quantitative analysis was made regarding ductility, affected both by porosity and the presence of Fe-rich phases.

Introduction

Semi-solid metal (SSM) processing presents numerous advantages over conventional casting routes, including grain refinement, reduced porosity, improved mechanical properties, better die life in high pressure die-casting (HPDC) due to pouring at a lower temperature and near net shapes [1,2]. As one of the variations of SSM, RheoMetal^{TM} process enables the production of slurry within 30 seconds and can be included in an HPDC route without significant adjustments, which makes the process promising in industrials.

During the process of SSM, the rheological properties of the slurry directly affect events during filling process and subsequently influence the microstructure of castings. A slurry with small and globular particles can minimize the formation and severity of defects, including shear band and porosity [3]. Santos [4] found that particle clusters play a strong role in the formation of shear bands. Payandeh [5] found that the liquid segregation bands and shear bands strongly affect the fracture behavior and elongation. Therefore, how to sufficiently stir the slurry to produce homogeneously distributed small round particles is crucial to improve the mechanical properties of castings. Previous study mainly focused on optimizing the morphology of primary α-Al particles. Generally, increased stirring speed [6] and intensity [7] produce smaller and more globular primary particles, while increased stirring time may cause an increase in the primary particle size [8]. However, how to effectively activate the slurry with a homogeneous distribution of α-Al particles was rarely studied, even though it is decisive in the formation of defects. Moreover, the migration of solid particles towards the central region during the filling process is common due to the high mobility of the particles, forming surface liquid segregation (SLS) layer [9]. However, the typical solid fraction of the slurry used in RheoMetal^{TM} process is around 0.4, falling in the range of the dendritic coherency point solid fraction (varying from 0.15 to 0.5, depending on particle size and shape) where the slurry starts to present a yield strength as the particles touch with each other [10]. Therefore, it is possible to minimize the formation of the SLS layer at the most extent by stirring the slurry and distributing particles homogeneously.

In this study, an optimized stirrer with two blades was used to stir and activate the slurry. Activating slurry with previously used stirrers (naked rod), as a reference, was also performed. The influence of both two stirrers on the microstructure and mechanical properties of castings was studied.

Experimental

Slurry preparation and casting. The chemical composition of the Magsimal 59 alloy used in this study is listed in Table 1. The RheoMetal^{TM} [11] process was used for slurry preparation, with constant stirring speed and melt temperature, around 1100 rpm and 660 ºC (38 ºC of superheat) respectively. The slurry was stirred by two types of stirrers with a range of stirring time for 14, 18, and 22 s. A schematic of the stirrers is shown in Fig. 1. The weight of the Enthalpy Exchange Material (EEM) was set as 6 pct of the shot weight. The EEM was preheated up to 200 ºC before slurry preparation. Subsequently, the slurry was cast by 50 tons vertical pressure die casting (VPDC) machine to produce bars in 10 mm thickness. The die temperature was controlled by a PolyTemp HTF 300 heater with the temperature at 175 ºC. Plunger speed kept constant at ~0.4 m/s. Before semi-solid casting, 5 liquid shots were performed to heat the machine and maintain the thermal conditions in the shot sleeve and die cavity.

Table 1. Chemical composition of Magsimal 59 alloy [wt. %].

Al	Si	Fe	Cu	Mn	Mg	Zn	Ti
Bal.	1.8-2.6	0.2	0.03	0.5-0.8	5.0-6.0	0.07	0.2

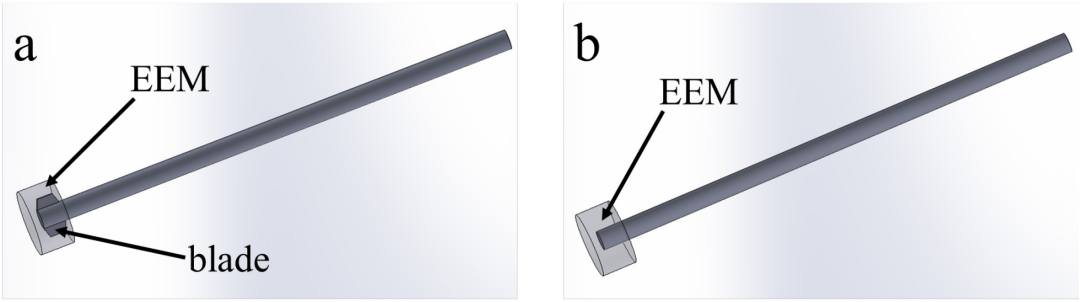

Fig. 1. Schematic of the stirrer, (a) for intensive stirring; (b) for regular stirring.

Tensile testing. 5 tensile bars were tested for each condition and no surface treatment/machining was performed on the samples. The tensile bars were tested according to the SS-EN ISO 6892-1:2016 using a Zwick/Roell Z100 machine with a constant strain rate of 0.00025s^{-1} up to offset yield strength determination and subsequently a faster strain rate of 0.002 s^{-1} until fracture. A LaserXtens extensometer was used to measure the elongation.

Microstructure characterization. The metallographic samples were prepared by standard metallographic procedures. For optical microscopy, a 10% NaOH solution was used to better characterize the primary α-Al particles. The castings in section B (with a length of 60 mm) were cut evenly into 12 pieces along transverse cross-section for the determination of the area fraction of porosity and the characterization of microstructures by optical microscopy (Olympus GX71F). The whole area of pores on each transverse cross-section was measured and then divided by the area of cross-section. To determine solid fraction, the micrographs along central line on each cross-section were measured at a magnification of 200. Scanning electron microscopy (JEOL JSM-7001F SEM) equipped with Energy-dispersive X-ray spectroscopy (EDS) was used to determine the proportion of Fe-rich phase. Due to the small size of Fe-rich intermetallic, 25 micrographs with a higher magnification of 500 were taken randomly from central part of the cross-section to assess the Fe-rich intermetallic for each sample.

The fracture surfaces after tensile test were analyzed with SEM and EDS to evaluate the fracture mode and the area fraction of porosity on the fracture surface. EDS maps on 3 central regions at a magnification of 150 were performed to quantify the area fraction of Fe-rich phase on fracture surface for each sample.

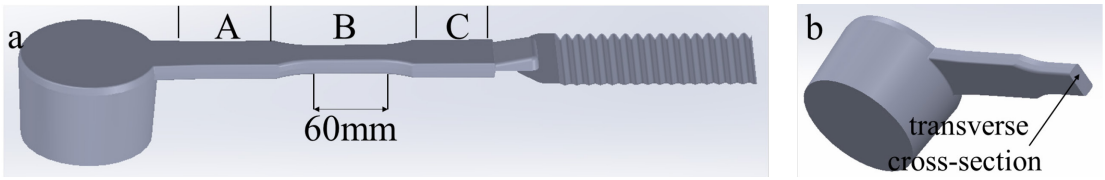

Fig. 2. Casting sample a) and the transverse cross-section b) for metallographic study.

Results and Discussion

Microstructural characterization. Table 2 shows that intensive stirring slightly reduces the primary α-Al particle size, indicating that the intensive stirring can break up the particles into small ones. Besides, samples under intensive stirring show an overall higher solid fraction, ranging from 2.2% to 4.4%. Li [12] reported that oxide formed in Al-Mg alloys is $MgAl_2O_4$ which can act as potent sites for nucleation of α-Al grain. Intensive stirring increases the number density of $MgAl_2O_4$ particles due to forced dispersion, promoting the formation of α_2-Al particles during filling process, as shown in Fig. 3b. As a result, the solid fraction increases. Dahle reported that during filling and solidification process, pores will form when partially solid slurry fractures at high solid fraction, due to the lack of liquid to compensate [13]. Therefore, higher solid fraction, especially accompanied with the presence of small α_2-Al particles which decreases the permeability of the slurry [14], leads to higher porosity in samples with intensive stirring, as shown in Table 4.

Table 2. Characters of primary α-Al particles and solid fraction.

Stirring time [s]		14	18	22
Particle size [μm]	Regular stirring	58±4	60±4	58±3
	Intensive stirring	56±2	58±4	55±3
Solid fraction [%]	Regular stirring	58±2	59±3	60±2
	Intensive stirring	63±2	61±2	62±3

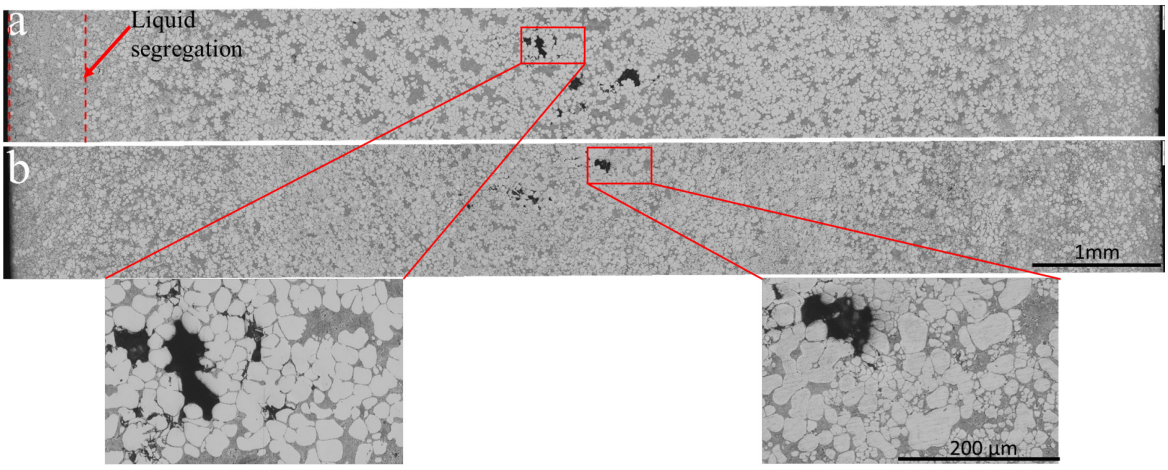

Fig. 3. Microstructure of castings, a) regular stirring and b) intensive stirring for 22 s.

Fig. 3 shows the microstructure across the longitudinal cross-section of tensile bars under different casting conditions. As seen in Fig. 3 (a), more particle clusters exist in regular stirring samples which interlock with each other, forming many closed large eutectic zones and pores, depending on if there is sufficient liquid to compensate. In contrast, fewer large pores are found in intensive stirring samples, Fig. 3 (b), probably due to the absence of particle clusters. However, the presence of the small α_2-Al particles decreases the permeability of the slurry, resulting in an increased number of small pores. Consequently, an increased overall porosity is presented, Table 2. Besides, an obvious SLS layer is also observed in the regular stirring samples. It is clear that intensive stirring breaks up particle clusters and distributes particles more homogeneously. The dispersed particles are likely to form a network where the particles touch with each other across the whole section. As a result, the

thickness of SLS layer reduces significantly due to the reduced mobility of the particles during the filling process.

The morphology of the Fe-rich intermetallic is shown in Fig. 4. With increased stirring time the Fe-rich intermetallic become slightly coarser for both stirring conditions. Moreover, the Fe-rich intermetallic in samples with intensive stirring are significantly coarser. The coarser intermetallic is the result of the dissolution of iron from the stainless-steel blades in the stirrers. More iron can be dissolved into the melt with the increased stirring time, Table 4, forming coarse intermetallic.

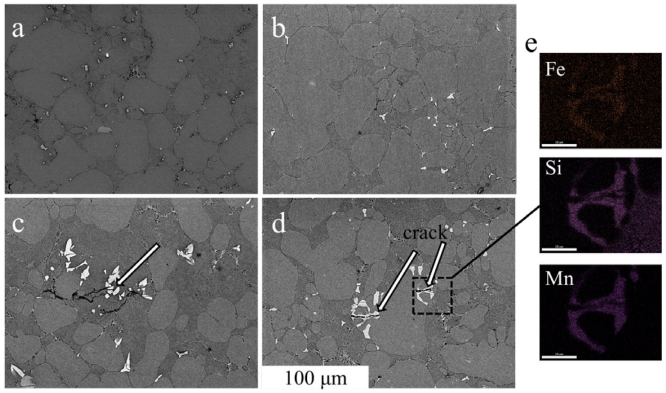

Fig. 4. Micrographs of the Fe-rich intermetallic in samples with regular stirring for a) 14 s and b) 22 s, and intensive stirring for c) 14 s and d) for 22 s; e) EDS map of Fe-rich metallic in d).

Mechanical properties. The tensile test results are shown in Table 3. The samples with regular stirring show higher elongation than samples with intensive stirring, indicating that the Fe-rich phase and porosity determine the ductility property while the influence of both morphologies of primary α-Al particles and homogeneousness of microstructure are negligible.

Table 3. Elongation value of samples under various conditions [%].

Stirring time	14	18	22
Regular stirring	8.3±1.1	7.3±0.9	7.3±0.9
Intensive stirring	5.9±1.8	6.9±1.5	5.5±1.2

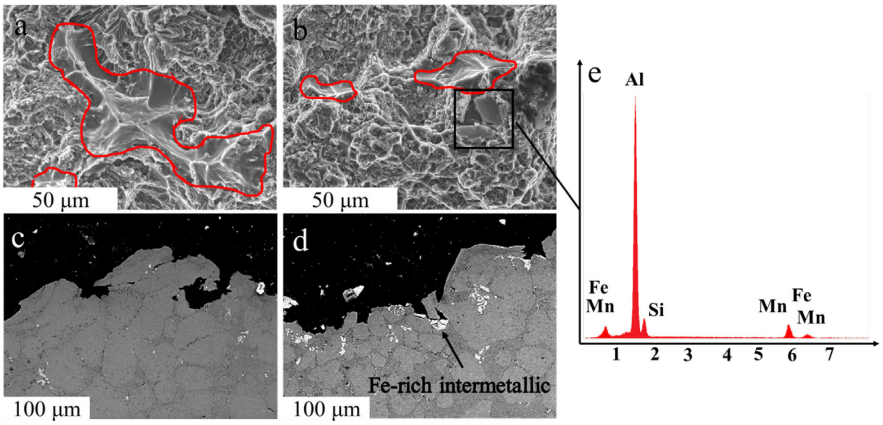

Fig. 5 Fracture surface and section profile, (a), (c) regular stirring for 14s, (b), (d) intensive stirring for 22s, and (e) EDS result of faceted surface in (b).

Fractographic examination. Fig. 5 (a) shows the fracture surface of samples with regular stirring for 14 s. As seen, a large fraction of ductile α-Al particles surrounded by dimpled structure were observed, which showed the ductile fracture characteristics. In samples with intensive stirring for 22 s, in addition to the dimples and a smaller fraction of ductile α-Al particles were found, cleavage planes were also observed, indicating that the fracture mode was mixed ductile-brittle fracture, Fig. 5 (b). EDS analysis shows that the cleavage plane is Fe-rich intermetallic, Fig. 5 (e). As seen in Fig. 5 (c), almost no Fe-rich intermetallic were found, while distinct plastic deformation of primary α-Al particles was observed in samples with regular stirring for 14 s. In contrast, many Fe-rich intermetallic accompanied with secondary cracks presented along the fracture profile of samples with

intensive stirring for 22 s. This is consistent with the observation of fracture morphology. In summary, compared with samples with regular stirring for 14 s, more Fe-rich particles present in samples with intensive stirring for 22 s, reducing the elongation due to the brittle nature of Fe-rich particles.

Quantitative analysis was carried out to identify the predominant effect of porosity and Fe-rich intermetallic on the elongation, in Table 4. The samples with regular stirring show a lower and stable proportion of both porosity and Fe-rich intermetallic. Both these factors have a detrimental effect on the ductility. While the samples with intensive stirring show an increased fraction of Fe-rich intermetallic, especially for the samples stirred for 22s, leading to a sharp drop in elongation. To further assess the individual effect of both porosity and Fe-rich intermetallic on the elongation, the Ratio of the fraction on fracture surface to fraction within samples was introduced for both porosity (R_p) and Fe-rich intermetallic (R_i). It is obvious that the R_p of regular stirring samples are significantly higher than intensive stirring samples, even though the fracture generally initiates from the location with high porosity fraction for both intensive stirring conditions, as shown in Fig. 6. This is probably because in normal stirring samples the porosity dominates the locations where fractures occur due to higher stress and the crack propagates along the pores, rather than Fe-rich intermetallic. In contrast, for the intensive stirring samples, the fractures locate at regions with higher porosity while show less porosity fraction on the fracture surface. This indicates that the porosity predominates the fracture locations, while the Fe-rich intermetallic instead of pore determine the crack propagation, Fig. 5(d). Moreover, the overall higher R_i of intensive stirring samples also confirms that the cracks are prone to across the Fe-rich intermetallic.

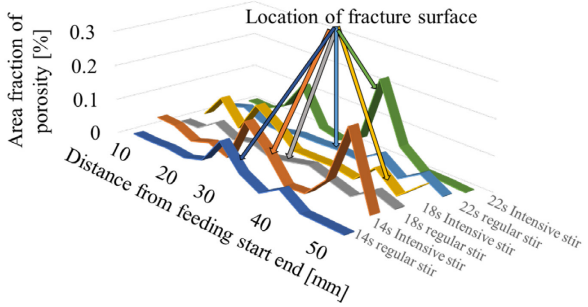

Fig. 6. Distribution of porosity across samples and the location of fracture.

Table 4. Porosity and Fe-rich intermetallic in samples and fracture surface [area percentage, %].

Stirring time [s]		Porosity			Fe-rich intermetallic		
		14	18	22	14	14	22
Within samples	Regular	0.02±0.02	0.02±0.01	0.02±0.01	0.42±0.05	0.44±0.16	0.42±0.09
	Intensive	0.06±0.04	0.04±0.02	0.04±0.04	0.47±0.08	0.52±0.10	0.74±0.19
Fracture surface	Regular	11.4±10.1	5.7±8.0	3.9±5.1	0.43±0,05	0.67±0.08	0.82±0.54
	Intensive	4.7±4.4	4.1±6.8	3.0±5.7	0.94±0,84	1.33±0.54	2.22±0.84
Ratio	Regular	633.33	258.18	206.84	1.02	1.52	1.96
	Intensive	85.45	117.71	71.43	2.01	2.56	3.01

Conclusions

The following conclusions can be made:

- Intensive stirring could slightly reduce the primary α-Al particle size.
- Intensive stirring produces more α_2-Al particles during filling process probably due to the enhanced heterogeneous nucleation, which increases the solid fraction in Al-Mg alloys and also the permeability in the slurry. Consequently, more pores are formed in samples with intensive stirring due to lack of liquid to compensate the solidification shrinkage.
- Additional iron was dissolved into slurry from the blades during slurry preparation process. With increased stirring time, coarser and more Fe-rich intermetallic precipitates along the primary α-Al grain boundary.

- The combination of Fe-rich intermetallic and porosity dramatically reduces the elongation. For the sample with regular stirring, porosity dominates the crack path. With an increase amount of intermetallic, the cracks propagate across the intermetallic instead of pores in samples with intensive stirring.

Acknowledgment

The current work ReCKA was funded by Vinnova contract number 2018-02831.

References

[1] Z. Fan, Semisolid metal processing, Int. Mater. Rev. 47 (2003) 49–85.

[2] A. Pola, M. Tocci, P. Kapranos, Microstructure and properties of semi-solid aluminum alloys: A literature review, Metals (Basel). 8 (2018) 181.

[3] A.K. Dahle, S. Sannes, D.H. St. John, H. Westengen, Formation of defect bands in high pressure die cast magnesium alloys, J. Light Met. 1 (2001) 99–103.

[4] J. Santos, A.E.W. Jarfors, A.K. Dahle, Filling, feeding and defect formation of thick-walled AlSi7Mg0.3 semi-solid castings, Solid State Phenom. 256 (2016) 222–227.

[5] M. Payandeh, A.E.W. Jarfors, M. Wessén, Influence of Microstructural Inhomogeneity on Fracture Behaviour in SSM-HPDC Al-Si-Cu-Fe Component with Low Si Content, Solid State Phenom. 217–218 (2014) 67–74.

[6] M. Reisi, B. Niroumand, Effects of stirring parameters on rheocast structure of Al-7.1wt.%Si alloy, J. Alloys Compd. 470 (2009) 413–419.

[7] B.N. P. Melali, P. Ashtijoo, Effect of stirring speed and flow pattern on the microstructure of a rheocast Al-Mg alloy, Met. Mater. Eng. 21 (2015) 35–43.

[8] L. Ratke, A. Sharma, D. Kohli, Effect of process parameters on properties of Al-Si alloys cast by Rapid Slurry Formation (RSF) technique, in: IOP Conf. Ser. Mater. Sci. Eng., 2011.

[9] H.I. Laukli, C.M. Gourlay, A.K. Dahle, Migration of crystals during the filling of semi-solid castings, Metall. Mater. Trans. A. 36 (2005) 805–818.

[10] C.M. Gourlay, A.K. Dahle, Dilatant shear bands in solidifying metals, Nature. 445 (2007) 70–73.

[11] M. Wessén, H. Cao, The RSF technology-A possible breakthrough for semi-solid casting processes, Int. Conf. High Tech Die Cast. (2006) 22–28.

[12] H.-T. Li, Y. Wang, Z. Fan, Mechanisms of enhanced heterogeneous nucleation during solidification in binary Al–Mg alloys, Acta Mater. 60 (2012) 1528–1537.

[13] A.K. Dahle, D.H. StJohn, Rheological behaviour of the mushy zone and its effect on the formation of casting defects during solidification, Acta Mater. 47 (1998) 31–41.

[14] J. Wang, J. Zhao, Y. Zhang, D. Wang, Y. Li, Y. Song, Analysis of the effect of particle size on permeability in hydrate-bearing porous media using pore network models combined with CT, Fuel. 163 (2016) 34–40.

The publication of this article was funded by the KTH Royal Institute of Technology 10.13039/501100004270